

# Repository of the Max Delbrück Center for Molecular Medicine (MDC) in the Helmholtz Association

https://edoc.mdc-berlin.de/15937

# Brain iron accumulation in Wilson disease: a post-mortem 7 Tesla MRI - histopathological study

Dusek, P., Bahn, E., Litwin, T., Jablonka-Salach, K., Luciuk, A., Huelnhagen, T., Madai, V.I., Dieringer, M.A., Bulska, E., Knauth, M., Niendorf, T., Sobesky, J., Paul, F., Schneider, S.A., Czlonkowska, A., Brueck, W., Wegner, C., Wuerfel, J.

This is the final version of the accepted manuscript. It is the peer reviewed version of the following article:

P. Dusek, E. Bahn, T. Litwin, K. Jabłonka-Salach, A. Łuciuk, T. Huelnhagen, V. I. Madai, M. A. Dieringer, E. Bulska, M. Knauth, T. Niendorf, J. Sobesky, F. Paul, S. A. Schneider, A. Czlonkowska, W. Brück, C. Wegner and J. Wuerfel (2017) Neuropathology and Applied Neurobiology 43, 514–532 Brain iron accumulation in Wilson disease: a post mortem 7 Tesla MRI – histopathological study

which has been published in final form in:

Neuropathology and Applied Neurobiology 2017 SEP 12; 43(6): 514-532

2016 OCT 04 (first published online: final publication)

doi: 10.1111/nan.12341

Publisher: Wiley-Blackwell

Copyright © 2016 British Neuropathological Society

This article may be used for non-commercial purposes in accordance with Wiley Terms and Conditions for Self-Archiving.

Received Date: 01-Jun-2016
Revised Date: 02-Aug-2016
Accepted Date: 18-Aug-2016
Article type: Original Article

Brain iron accumulation in Wilson disease: a post-mortem 7 Tesla MRI - histopathological study

Petr Dusek<sup>1,2</sup>, Erik Bahn<sup>3</sup>, Tomasz Litwin<sup>4</sup>, Katarzyna Jabłonka-Salach<sup>5</sup>, Anna Łuciuk<sup>5</sup>, Till Huelnhagen<sup>6</sup>, Vince Istvan Madai<sup>7</sup>, Matthias A Dieringer<sup>6,8</sup>, **Ewa Bulska<sup>5</sup>**, Michael Knauth<sup>1</sup>, **Thoralf Niendorf<sup>6,8</sup>**, Jan Sobesky<sup>7,8</sup>, **Friedemann Paul<sup>8,9</sup>**, **Susanne A Schneider<sup>10,11</sup>**, **Anna Czlonkowska<sup>4,12</sup>**, **Wolfgang Brück<sup>3</sup>**, **Christiane Wegner<sup>3\*</sup>**, and Jens Wuerfel<sup>1,9,13\*</sup>

<sup>1</sup>Institute of Neuroradiology, University Medical Center Göttingen, Göttingen, Germany

<sup>2</sup>Department of Neurology and Center of Clinical Neuroscience, Charles University in Prague, 1<sup>st</sup> Faculty of Medicine and General University Hospital in Prague, Praha, Czech Republic

<sup>3</sup>Institute of Neuropathology, University Medical Center Göttingen, Göttingen, Germany

<sup>4</sup>2<sup>nd</sup> Department of Neurology, Institute Psychiatry and Neurology, Warsaw, Poland

<sup>5</sup> Faculty of Chemistry, Biological and Chemical Research Centre, University of Warsaw, Warsaw, Poland

<sup>6</sup>Berlin Ultrahigh Field Facility (B.U.F.F.), Max-Delbrück Center for Molecular Medicine in the Helmholtz Association, Berlin, Germany

<sup>7</sup>Department of Neurology and Center for Stroke Research Berlin (CSB), Charité-Universitätsmedizin, Berlin, Germany

<sup>8</sup>Experimental and Clinical Research Center (ECRC), Charité-Universitätsmedizin and Max Delbrück Center for Molecular Medicine (MDC), Berlin, Germany

<sup>9</sup>NeuroCure Clinical Research Center and Clinical and Experimental Multiple Sclerosis Research Center, Department of Neurology, Charité-Universitätsmedizin, Berlin, Germany

<sup>10</sup>Neurology Department, University of Kiel, Kiel, Germany

<sup>11</sup>Department of Neurology, Ludwig-Maximilians-University, Munich, Germany

<sup>12</sup>Department of Experimental and Clinical Pharmacology, Medical University, Warsaw, Poland

This article has been accepted for publication and undergone full peer review but has not been through the copyediting, typesetting, pagination and proofreading process, which may lead to differences between this version and the Version of Record. Please cite this article as doi: 10.1111/nan.12341

This article is protected by copyright. All rights reserved.

<sup>13</sup>Medical Imaging Analysis Center AG, Basel, Switzerland

\*C.W. and J.W. share co-senior authorship

Correspondence to:

Petr Dusek

Department of Neurology and Center of Clinical Neuroscience

Charles University in Prague

1st Faculty of Medicine and General University Hospital in Prague

Katerinska 30, 120 00, Praha 2, Czech Republic

E-mail: pdusek@gmail.com

Phone: (+420) 224 965 528

Running title: Wilson and iron

Keywords: Wilson disease; iron accumulation; post-mortem 7T MRI; pathology; brain

# Abstract

Aims: In Wilson disease (WD), T2/T2\*-weighted (T2\*w) MRI frequently shows hypointensity in the basal ganglia that is suggestive of paramagnetic deposits. It is currently unknown whether this hypointensity is related to copper or iron deposition. We examined the neuropathological correlate of this MRI pattern, particularly in relation to iron and copper concentrations.

Methods: Brain slices from nine WD and six control cases were investigated using a 7T-MRI system. High resolution T2\*w images were acquired and R2\* parametric maps were reconstructed using a multi-gradient recalled echo sequence. R2\* was measured in the globus pallidus (GP) and the putamen. Corresponding histopathological sections containing the lentiform nucleus were examined using Turnbull iron staining, and double staining combining Turnbull with immunohistochemistry for macrophages or astrocytes. Quantitative densitometry of the iron staining as well as copper and iron concentrations were measured in the GP and putamen and correlated to R2\* values.

Results: T2\*w hypointensity in the GP and/or putamen was apparent in WD cases and R2\* values correlated with quantitative densitometry of iron staining. In WD, iron and copper concentrations were increased in the putamen compared to controls. R2\* was correlated with the iron concentration in the GP and putamen whereas no correlation was observed for the copper concentration. Patients with more pronounced pathological severity in the putamen displayed increased iron concentration, which correlated with an elevated number of iron-containing macrophages.

Conclusions: T2/T2\*w hypointensity observed in vivo in the basal ganglia of WD patients is related to iron rather than copper deposits.

**Abbreviations:** GP = globus pallidus, MP-RAGE = magnetization-prepared rapid acquisition gradient echo, GRE = gradient echo, DAB = 3,3'-diaminobenzidine-tetrahydrochloride, CN = caudate nucleus, ROI = region of interest, ICP-MS = inductively coupled plasma mass spectrometry, AAS = atomic absorbption spectroscopy, PKAN = pantothenate kinase-associated neurodegeneration, SWI = susceptibility weighted imaging

### Introduction

Wilson disease, formerly referred to as hepatolenticular degeneration, is a genetic disorder caused by mutation of *ATP7B* copper transporter. This defect leads to gradual accumulation of copper in the body and reduced synthesis of ceruloplasmin [1]. Neurologic symptoms are presumably caused by copper toxicity and are typically associated with distinct neuropathological abnormalities. They mostly affect the basal ganglia and the brainstem. A soft, brownish, atrophic putamen with cavitations is a characteristic finding at macroscopic examination. Microscopic evaluation frequently shows a varying degree of tissue loss in the basal ganglia. It ranges from mild rarefaction with spongy degeneration and microcavitation to large-scale necrosis with the infiltration of macrophages causing formation of a cystic cavity that affects the entire putamen [2-4]. These degenerative changes are associated with marked astrocytic abnormalities including astrogliosis with large, swollen, multinucleated astrocytes and the presence of enlarged forms with large pale nuclei referred to as type I and type II Alzheimer glia [5].

Brain MRI in Wilson disease typically shows increased signal intensity in the basal ganglia, thalamus, and brainstem on T<sub>2</sub>-weighted (T<sub>2</sub>w) images which is likely due to tissue edema, cavitation, myelin loss and/or gliosis. Longitudinal neuroimaging studies demonstrated a partial recovery of the T<sub>2</sub>w hyperintense signal in the majority of Wilson disease patients who received treatment [6]. Furthermore, decreased signal intensity in the basal ganglia on T<sub>2</sub>w images and/or a shift in frequency on susceptibility weighted images (SWI) have also been described in Wilson disease [7-12]. This abnormality, particularly present in the lentiform nucleus (globus pallidus [GP] and putamen), apparently worsens during the disease course [13] and is suggestive of paramagnetic metal deposits that cause irregularity in the local magnetic field and subsequent MR signal loss. It has been argued that these deposits could be formed either by certain copper species with paramagnetic properties [14] or by iron compounds [7]. Currently, it is, however, not known whether and to what extent copper ions can affect the tissue MRI signal [15, 16].

Post-mortem brain tissue examinations in Wilson disease cases document an up to 10-fold increase in copper concentration compared to controls [17-19]. Abnormal brain copper deposits could be detected even after several years of chelation treatment and correlated fairly well with the severity of tissue destruction [20]. A few post-mortem case studies also examined cerebral iron content in Wilson disease [18, 21, 22]. A study of 12 Wilson disease cases reported increased iron content in the dentate nucleus [17]. In addition to post-mortem examinations, *in vivo* positron emission tomography with radioactively labeled iron also showed increased net brain iron uptake in Wilson disease patients compared to healthy volunteers [23]. Notably, previous studies examining iron

concentration in Wilson disease did not focus on the lentiform nucleus, where the signal drop is typically present on  $T_2/T_2*w$  MRI in vivo.

The goal of this study was to investigate the neuropathological correlate of hypointensities on  $T_2/T_2$ \*w MRI in *post-mortem* Wilson disease brain tissue.

#### Materials and methods

### Study design and sample characteristics

Brain samples from nine Wilson disease patients (seven with neuropsychiatric and two with hepatic symptoms; Table 1) and six control subjects (Table 2) were investigated. This study was approved by the local ethics committee. Formalin-fixed brains, cut into 10-15 mm coronal slices, were obtained from the Department of Neuropathology, Institute of Psychiatry and Neurology, Warsaw, Poland and the Institute of Neuropathology, University Medicine Göttingen, Germany. Wilson disease was confirmed according to the Leipzig diagnostic criteria [24] and the American Association for Study of Liver Diseases (AASLD) recommendations [25], which require typical clinical and neuroimaging findings, Kayser-Fleischer ring, low serum ceruloplasmin, and high 24-hour urine copper excretion. In two patients, Wilson disease diagnosis was additionally confirmed by genetic examination (Table 1). All Wilson disease cases with neuropsychiatric manifestation except one (case 6) deteriorated during the disease course despite being on chelation therapy, and ultimately died due to complications of immobilization. Both hepatic cases died from liver failure. Liver cirrhosis was confirmed in all Wilson disease cases on autopsy. Control cases had no history of neurological diseases or evidence of pathology upon neuropathological examination.

# MR Image acquisition

Coronal brain slices containing the basal ganglia from nine Wilson disease patients and one control case were scanned while embedded in 4% formaldehyde solution in a plastic container using a 7T whole-body MRI system (Magnetom, Siemens Healthcare, Erlangen, Germany). A quadrature birdcage volume coil was used for transmission in conjunction with a 24 channel receive head RF coil array (Nova Medical, Wilmington, MA, USA). Brain samples were kept at room temperature (airconditioned room, 23°C) for several hours before scanning to achieve standard thermal conditions for relaxation time measurements [26].

For visual analysis, high spatial resolution images covering whole brain slices were acquired using the following pulse sequences:  $T_2$ \*weighted 3D double-echo gradient echo (GRE) (TR=50 ms, TE=6.1 and 19 ms,  $\alpha$ =15°, pixel bandwidth=148 Hz, spatial resolution 0.15x0.15x0.5 mm³, 7 averages, scan-time 01:31 h) and magnetization prepared rapid acquisition gradient echo (MP-RAGE) (TR=2300 ms, TE=5.9 ms,  $\alpha$ =15°, TI= 700ms, pixel bandwidth=148 Hz, spatial resolution 0.1x0.1x0.5 mm³, 15 averages, scan-time 2:36 h).

For  $T_2^*$  parametric mapping, a single image slice, that was chosen as 1) it was the best depiction of the putamen and the GP, and 2) it showed the most pronounced hypointensity on the high-resolution images, was acquired using a 2D multi-echo GRE pulse sequence (TR=500 ms,  $\alpha$ =35°, 8 equidistant echoes ranging from 4.6 to 47.2 ms, pixel bandwidth=260 Hz, spatial resolution 0.5x0.5x2.0 mm³, 32 averages, scan-time 0:35 h).

# Image reconstruction and analysis

For the high spatial resolution MP-RAGE and GRE images, a slight intensity homogenization was applied to compensate for spatial coil sensitivity variations [27]. Subsequently, the images were denoised employing a spatially adaptive non-local means filter [28] as implemented in the VBM8 (http://dbm.neuro.uni-jena.de/vbm8/) toolbox of the SPM package (http://www.fil.ion.ucl.ac.uk/spm/). The presence of abnormal hypointensities was confirmed on the MP-RAGE and the GRE image from the first echo acquisition.

 $T_2^*$  parametric maps were reconstructed from the multi-echo GRE images using the Levenberg–Marquardt curve-fitting algorithm in conjunction with a mono-exponential decay model as implemented in the MRI processor plugin (Dimiter Prodanov, 2009) for ImageJ (NIH, MD, USA) [29]. Reciprocal value  $R_2^*=1/T_2^*$  representing transverse relaxivity was calculated. On these parametric maps, we measured  $R_2^*$  values in regions of interest (ROI) drawn manually in areas with the most pronounced hypointensity in the GP and putamen and in an area covering the whole caudate nucleus (CN).

# Neuropathological examination

Following MRI examination, we collected tissue blocks from the following ROI: frontal lobe, insular region, lentiform nucleus, CN, pons, and mesencephalon. These samples were embedded in paraffin and sliced with a microtome into 5  $\mu$ m thick sections, which were stained with hematoxylin and eosin, and 3,3'-diaminobenzidine-tetrahydrochloride (DAB) enhanced Turnbull staining for Fe<sup>2+</sup> and Fe<sup>2+/3+</sup> iron as described previously [30, 31].

Immunohistochemistry was performed using primary antibodies to detect ferritin, macrophages, and astrocytes. Pretreatment as well as primary and secondary antibody incubation were carried out according to a standard protocol. The following primary antibodies were used: rabbit anti-ferritin (dilution 1:1000; Sigma, St.Louis, MO), mouse anti-KiM1P (dilution 1:5000) for macrophages, as well as mouse and rabbit anti-glial fibrillary acidic protein (GFAP; dilution 1:1000; Dako, Glostrup, Denmark) for astrocytes. Bound antibodies were visualized using an avidin-biotin technique with DAB as chromogen. Sections were briefly counterstained with Mayer's hemalum solution.

To examine the colocalization of iron with cell-type specific markers on sections from the lentiform nucleus, we performed double-labeling combining immunohistochemistry for macrophages or astrocytes with enhanced Turnbull staining. These Turnbull stainings used 3-amino-9-ethylcarbazole (AEC) as chromogen while alkaline phosphatase-anti alkaline phosphatase (APAAP; Dako) was employed for the visualization of primary antibody (anti-KiM1P and anti-GFAP) with Fast Blue as chromogen.

# Morphometry and semiquantitative analysis of neuropathological findings

The density of cells double stained by Turnbull and KiM1P (iron-containing macrophages) as well as cells double stained by Turnbull and GFAP (iron-containing astrocytes) was quantified in the putamen and GP using a 40x objective with 10x10 counting grid. To obtain median cell counts per 1 mm² we performed manual counts within ten visual fields to calculate the densities per cases. The degree of tissue disruption in the putamen and GP was evaluated semiquantitatively based on the level of rarefaction, disruption of myelin bundles and neuronal loss as none (-), mild (+), medium (++)

and severe (+++). Tissue disruption graded as "-" or "+" was regarded as mild, and "++" or "+++" as severe pathology in further analyses.

# Matching of MRI and histopathology

Digital images of Turnbull and ferritin-stained sections from the lentiform nucleus were taken using the Olympus dotSlide 2.1 digital scanning system. Overview images were compared side by side with the appropriate high-resolution GRE and MP-RAGE MRI slices to determine possible matching between the intensity of Turnbull and ferritin stainings and the degree of MR hypointensity.

To correlate the  $R_2^*$  parameter with the intensity of iron staining, quantitative densitometry of the Turnbull staining in ROIs from the putamen, GP, and CN sections was performed. High power (200x) images were obtained using a BX51 Olympus light microscope equipped with a DP71 digital camera, and the DAB channel was separated using the color deconvolution plugin for ImageJ [32]. Afterwards, 8-bit grayscale images were inverted and thresholded so that only gray values above 234/255, representing the most intense staining, were segmented. An index representing the proportion of tissue with positive Turnbull signal was defined as area fraction reflecting the percentage of pixels with an intensity above 234 (Suppl. Fig. 1). Measurements were averaged across five images per ROI.

#### Metal concentration measurement

Tissue specimens (each approximately 2x2x2 mm<sup>3</sup>) from all Wilson disease and control cases were collected using a ceramic knife to avoid metal contamination. The following regions were sampled: frontal cortex, insular cortex, GP, putamen, CN, pontine tegmentum, dentate nucleus and substantia nigra. Specimens were taken at identical locations from the same hemisphere as samples for histopathological examination. Specimens from the GP and putamen were taken from the location with the most pronounced hypointensity on MR images.

Brain specimens were left in a mixture of 2 ml of 65% nitric acid (Merck, Germany) and 10  $\mu$ L of 70% perchloric acid (Merck, Germany) for at least 15 hours at room temperature. The samples were then kept in an ultrasonic bath at 50 °C for three hours. Next, the solutions obtained were diluted with distilled water. To prevent the clogging of inductively coupled plasma mass spectrometry (ICP-MS) tubes, diluted samples were filtered using polyvinylidene fluoride (PVDF) syringe filters with a pore size of 0.45  $\mu$ m. Copper concentration was analyzed using ICP-MS (NexION 300D, PerkinElmer, USA); the <sup>63</sup>Cu and <sup>65</sup>Cu isotopes were monitored. Because of potential isobaric interference in measurement of iron isotopes using ICP-MS, iron concentration was analyzed using flame atomic absorption spectroscopy (ContrAA 700, Analytik Jena, Germany). Iron was monitored at 248.3 nm and air-acetylene flame was used as an atomizer. The accuracy and overall performance of the analysis were verified using the following certified reference materials: Bovine Liver 1577c, NIST; LUTS-1, NRC-CNRC; Cod Muscle BCR 422; Mussel Tissue SRM 2976, NIST. Mili-Q water (Milipore, USA) was used for all samples and standard procedures. The results are presented as the mean of three consecutively repeated measurements of each sample and concentrations are expressed as  $\mu$ g/g fixed wet weight.

#### **Statistics**

Group differences were tested using the non-parametric Mann-Whitney U test. Dependencies of variables were assessed using Pearson correlation coefficients after tested values passed the D'Agostino-Pearson normality test. Correlations are expressed as  $r^2$  (R squared). P-values <0.05 (two-tailed) were considered significant. Statistical evaluations and graph plots were performed using GraphPad Prism version 6 (GraphPad Software, Inc., San Diego, CA, USA). Additionally, a hierarchical multivariate linear regression analysis to calculate independent effects of iron and copper concentrations on R2\* value was performed using SPSS version 22 (Armonk, NY, IBM Corp.).

#### Results

# Comparison of MRI and histopathology

First, we examined the high resolution GRE and MP-RAGE MR images for the presence of abnormal hypointensities in the basal ganglia and matched them visually with the intensity of iron staining. Compared to control cases, abnormally hypointense signals suggestive of paramagnetic deposits were observed in the GP and/or the putamen of all seven Wilson disease cases with neuropsychiatric presentation (neuro-WD). Two neuro-WD cases displayed an only slightly hypointense signal in the CN. No signal alterations were detected in the two cases with hepatic presentation (hepato-WD). The appearance and extent of hypointensities were similar for MP-RAGE and GRE images. The Turnbull staining was positive only when Fe<sup>2+/3+</sup> iron was stained, while there was virtually no Fe<sup>2+</sup> iron staining. This is consistent with the vast predominance of Fe<sup>3+</sup> iron in post-mortem tissue [31, 33]. On visual inspection, the intensity of the Turnbull staining (here and further in the text Turnbull refers to the Fe<sup>2+/3+</sup> iron staining) in the GP and putamen appeared to be closely matched with MR signal loss in the corresponding region (Fig. 1, Suppl. Fig. 2).

Upon neuropathological examination, Wilson disease subjects exhibited typical changes with the most severe tissue disruption seen in the putamen (Fig. 2A-F). The putamen displayed variable shrinkage and tissue changes ranging from mild astrogliosis, neuronal loss and rarefaction to severe cavitation with marked astrogliosis. At the edge and in the center of the cavitation a perivascular and diffuse infiltration by macrophages could be detected. Most of the reactive astrocytes showed enlarged vesicular nuclei and inconspicuous cytoplasm, indicating Alzheimer type II glia. Occasional large, sometimes multinucleated, astrocytic cells were also observed (Fig. 2E, F). Compared to the putamen, the tissue damage, cellular infiltration, and astrogliosis were considerably less pronounced in the GP and CN (Table 3).

The histological examination revealed dense Turnbull staining located predominantly in phagocytic cells (Fig. 2C) in the areas with MR signal loss. The ferritin immunostaining matched very closely the Turnbull iron staining, which was also predominantly positive in phagocytic cells (Fig. 2D). MR signal loss was even detected in cases with profound tissue rarefaction where deposits with dense iron staining and ferritin positivity were present. This finding suggests that these iron deposits composed of aggregated ferritin are likely to be the principal source of local magnetic field inhomogeneity in the lentiform nucleus. Very few dense iron deposits were observed in the CN.

# Iron localization in the lentiform nucleus

To determine the cellular source of iron deposits in the lentiform nucleus in Wilson disease, we performed standard histology as well as immunohistochemistry combined with Turnbull staining. In control cases, iron was observed mostly in oligodendrocytes and myelinated bundles passing through the putamen and GP. In neuro-WD cases, more intense iron staining with a different histological pattern of iron distribution was apparent. In contrast to controls, neuro-WD cases showed less iron in remaining myelinated bundles but displayed additional cellular, and to a lesser degree also apparently extracellular, iron deposits. The highest iron load was visible in numerous phagocytic cells and a few reactive astrocytes (Fig. 2C, D). Intracellular iron appeared as diffuse cytoplasmic deposits in many KiM1P+ macrophages (Fig. 2G) and as small cytoplasmic granules in a few reactive GFAP+ astrocytes (Fig. 2H).

Combining Turnbull with immunohistochemical staining for macrophages or astrocytes, quantitative analysis revealed that the number of iron-positive macrophages was higher than iron-positive astrocytes. The cellular infiltration by iron-positive KiM1P+ macrophages and GFAP+ astrocytes was more prominent in the putamen compared to the GP (Table 3).

# Correlation between R2\* parametric mapping and quantitative densitometry of iron staining

To assess the dependence of the MR signal loss and the intensity of dense iron particles we correlated the  $R_2^*$  value with the quantitative densitometry of the iron staining. The  $R_2^*$  value closely correlated with the proportion of tissue with positive Turnbull signal in the GP ( $r^2$ =0.57, p=0.02; Fig. 3A) and putamen ( $r^2$ =0.64, p=0.01; Fig. 3B), confirming that  $R_2^*$  is strongly influenced by dense iron deposits mainly located in macrophages. Quantitative densitometry yielded a very low proportion of tissue with positive Turnbull signal in the CN (Fig. 3C) in agreement with the observation of a low number of dense iron deposits in this region.

# Quantitative analysis of tissue metal content and its correlation with R2\* parametric mapping

Next, we quantitatively analyzed the concentration of iron and copper in control and Wilson disease tissue samples. In controls the highest iron concentration was found in the substantia nigra and the GP while the highest copper concentration was found in the substantia nigra and the dentate nucleus (Fig. 4, Suppl. Table 1) as reported previously [34]. Iron levels were higher in all analyzed brain regions in neuro-WD subjects compared to controls, but significant differences were only found in the putamen, CN, and pontine tegmentum. In contrast, cerebral iron levels were not increased in the hepato-WD cases. Copper levels were significantly increased by a factor of 5-10 in all analyzed brain regions in neuro-WD, and to a lesser degree in hepato-WD cases, compared to controls. In controls, a weak but significant inter-elemental correlation was observed between iron and copper concentrations when data from all examined brain regions were merged ( $r^2$ =0.19, p=0.002). In Wilson disease, the correlation between iron and copper concentrations was not significant ( $r^2$ =0.05, p=0.056; Suppl. Fig.3). A subanalysis in the basal ganglia (merged data from the GP, putamen, and CN) showed a significant correlation between iron and copper concentrations in control ( $r^2$ =0.63, p<0.0001) and Wilson disease ( $r^2$ =0.19, p=0.02) cases, respectively.

To assess the contribution of iron and copper to the  $T_2^*$  transverse relaxation of the tissue, we correlated the  $R_2^*$  value with metal concentrations in the entire Wilson disease group (hepato-WD and neuro-WD). Both hepato-WD cases were included to extend the range of values for the

correlation analysis by including tissue samples containing high copper and normal iron concentration.  $R_2^*$  values were significantly correlated with the iron concentration in the GP ( $r^2$ =0.77, p=0.002; Fig. 3D), putamen ( $r^2$ =0.80, p=0.001; Fig. 3E) and CN ( $r^2$ =0.49, p=0.03; Fig. 3F) while no significant correlations were observed for the copper concentration (Fig. 3G-I).

Additionally, a hierarchical multiple regression analysis was run to predict  $R_2^*$  values in the basal ganglia for either iron concentration alone (model 1) or for the combination of iron and copper concentrations (model 2). Iron concentration significantly predicted  $R_2^*$  value (F (1,25)=58.7, p<000.1,  $r^2$ =0.70). Adding copper concentration did not improve the prediction; in model 2, only iron concentration significantly contributed to the prediction of  $R_2^*$  value in the basal ganglia, whereby for every 1 µg/g of tissue iron concentration, the R2\* value was increased by 0.001 ms<sup>-1</sup> (Table 4).

# Correlation of metal content and neuropathological severity in the putamen

Finally, we aimed to examine whether iron accumulation in the putamen was an early or late feature of Wilson disease neuropathology. Therefore, we analyzed the dependence of iron and copper concentrations, the degree of tissue disruption and the density of iron-containing cells in the putamen. The degree of pathological severity in the putamen of Wilson disease cases revealed no association with copper concentration (p=0.73) while there was a trend for a positive association with iron concentration (p=0.06) (Suppl. Fig. 4).

The quantitative analysis showed that iron-positive macrophages and astrocytes were more abundant in the putamen of cases with more severe pathology (Fig. 5A, C). The number of iron-positive KiM1P+ macrophages was significantly correlated with the iron concentration ( $r^2$ =0.73, p=0.003; Fig. 5B), indicating that pathological iron deposits in the putamen are mainly caused by an increase in iron-containing macrophages. There was only a weak correlation between the number of iron-positive GFAP+ astrocytes and iron concentration in the putamen ( $r^2$ =0.41, p=0.06; Fig. 5D). In summary, iron accumulation seems to be a rather late event in the pathophysiological cascade, and neurodegeneration in the putamen in Wilson disease is apparently associated with a significant influx of iron-containing macrophages.

# Discussion

Our study shows i) that iron accumulates in the lentiform nucleus of Wilson disease patients with neuropsychiatric presentation and ii) that iron, but not copper, content in the putamen and GP correlates with the presence of hypointensities on  $T_2^*w$  MR images. Moreover, iron concentration and the degree of tissue disruption in the putamen are associated with the presence of iron-containing macrophages.

These findings are important for the interpretation of the MRI examination that frequently shows hypointensities on  $T_2/T_2*$ w and SWI images. Importantly,  $R_2*$  values cannot be used for brain copper content estimation and monitoring of anti-copper treatment. On the other hand, our results suggest that the development of putaminal  $T_2/T_2*$ w hypointensity in a Wilson disease patient indicates progressive degenerative changes and unfavorable prognosis. These findings may be helpful in the understanding of the pathophysiology of Wilson disease that apparently involves inflammatory changes.

Iron concentration in the neuropsychiatric Wilson disease group was higher in all examined brain areas compared to controls, but only reached significance in the putamen, caudate, and pontine tegmentum. A previous study on Wilson disease reported increased iron concentration in the dentate nucleus [17]. Our present study differs from this study in the use of MRI navigation for sampling; here, we were able to take samples directly from the regions showing the most prominent hypointensity. Apart from this, the disparate results between the two studies might be due to the high clinical heterogeneity in Wilson disease along with the small number of cases examined in each study. Indeed, the elevated iron concentration combined with prominent pathological changes in the putamen in our cases may be related to the fact that all of our neuropsychiatric WD cases presented with the dystonic subtype which has previously been associated with putaminal abnormalities [35]. Similarly to previous studies [34, 36], a significant correlation between regional cerebral iron and copper concentrations was found in control cases, suggesting a close relationship between metabolic roles of iron and copper under physiological conditions [37]. This correlation between iron and copper was not observed in Wilson disease, most likely due to the global cerebral copper accumulation that occurs in this disorder.

In our study, age at death of control subjects as well as fixation time of Wilson disease brains were higher than in the control group due to the scarcity of post-mortem material from Wilson disease patients and young healthy control subjects. Metals are prone to leach from fixated tissue during storage [38], and the content of iron in the brain increases with age [39]. The differences in age at death and fixation duration between Wilson disease and controls subjects, however, do not invalidate our findings of higher iron concentration in Wilson disease, since both of these parameters would bias the results towards a lower difference between the groups. It is likely that the true differences in iron content would be even more pronounced if Wilson disease and control cases were matched in an ideal way for age and fixation time in formalin.

The iron concentration was closely correlated with the  $R_2^*$  value in all examined regions, thus confirming that the MR signal loss is determined by iron species. On the microscopic level, the MR signal drop was associated with the presence of particles with a very intense iron and ferritin staining. This observation was confirmed by the positive correlation between  $R_2^*$  and the quantitative densitometry of the Turnbull staining that segmented the densest iron-positive particles. These particles, located predominantly in macrophages, may be composed of highly clustered ferritin or hemosiderin with strong paramagnetic properties. This is in agreement with an *in vitro* study showing that  $R_2$  transverse relaxivity of ferritin solution is proportional to the size of ferritin clusters under the condition of constant iron concentration [40]. Despite a significant increase in iron concentration in the CN, a mild  $T_2^*$ w hypointensity in this region was observed only in two Wilson disease cases. The moderate increase in iron concentration in the CN, which correlated with  $R_2^*$  value, together with a low number of dense iron particles were apparently not sufficient to cause a consistent  $T_2$ w hypointensity detectable with the applied MR parameters.

Although a weak correlation between the copper concentration and  $R_2^*$  value was observed, several factors suggest that copper does not significantly contribute to the MR signal loss in the lentiform nucleus. Adding copper concentration to the multiple regression analysis did not improve the prediction of  $R_2^*$  value in the basal ganglia compared to the analysis with iron concentration alone. Additionally, copper concentration in the cortex of all neuropsychiatric Wilson disease cases, and in the lentiform nucleus of both hepatic Wilson disease cases was increased to a level comparable to the lentiform nucleus of neuropsychiatric Wilson disease cases. Despite this, MR signal loss was not

observed in these structures. A previous case study documented that the area of T<sub>2</sub>w hypointensity increased during chelation treatment when cerebral copper concentration is thought to be decreasing [13]. Paramagnetic properties of copper species are not different in Wilson disease brain tissue compared to controls, as was shown by an electron spin resonance study [41]. It is thus likely that in Wilson disease, similarly to physiological conditions, copper is stored in a diamagnetic form bound to metallothionein, which is a protein involved in metal detoxification [42]. In contrast to a previous study [20] we did not observe any association between the copper concentration and the degree of pathological severity. Although the association between dose and toxicity in metal accumulation is evident *in vivo*, the interpretation of *post-mortem* measurements in severely affected tissue is not straightforward. Accumulated metals may gradually disappear from the rarefied tissue by drainage through extracellular space and phagocytosis.

Similar to physiological conditions, the iron concentration in Wilson disease subjects was highest in the GP and substantia nigra. While total iron concentration was not significantly increased in the GP, alterations in iron localization were apparent in this structure in the neuropsychiatric Wilson disease cases. In control cases, fine cytoplasmic iron granules were observed in oligodendrocytes, microglia, and in the perivascular extracellular space [43, 44]. In contrast, neuropsychiatric Wilson disease cases displayed additional iron deposits in macrophages and astrocytes. This observation, together with previous *in vivo* data [14, 45], suggests that iron metabolism in the GP may be disturbed at least in a subgroup of Wilson disease patients. Iron accumulation in the GP is a rather unspecific process observed in neurodegenerative diseases, inflammatory disorders, and aging [39, 46]. The reason for the propensity of the GP to accumulate iron and other metals is unclear. Several authors suggested that it could be related to cellular energy production failure in the brain [47], which may also be the case in Wilson disease since mitochondria are the principal targets of copper-mediated toxicity [48].

The putamen was the region with the most profound tissue disruption and significantly increased iron concentration. The MR signal drop in this area reflected the increased number of phagocytic cells densely packed with iron that were more abundant in the cases with more pronounced pathological changes. The association between neurodegeneration and the presence of iron-containing phagocytic cells seems to be common, but its causes and consequences are unclear [49, 50]. Macrophages may be attracted to phagocyte iron accumulated either due to damage of iron-rich oligodendrocytes and neurons or due to impairment of its transport across the disrupted blood-brain barrier. It has also been proposed that iron may be brought in by iron-containing phagocytic cells that migrate into the CNS as part of the inflammatory response that accompanies neurodegeneration [51].

Alternatively, iron may accumulate in astrocytes due to ceruloplasmin dysfunction inherent to Wilson disease. Since ATP7B is expressed in the brain [52], its dysfunction may lead to impaired production of ceruloplasmin in astrocytes, with the consequence of impaired cellular iron efflux similar to aceruloplasminemia [53]. Accordingly, studies on systemic iron metabolism in Wilson disease found increased serum ferritin and liver iron content [54-56]. The distribution of pathological changes in our Wilson disease cases was notably similar to aceruloplasminemia, showing the highest degree of tissue disruption and iron deposits in the putamen [57]. Also, iron is deposited in enlarged, deformed and multinucleated reactive astrocytes in both disorders [58]. On the other hand, iron accumulation in astrocytes is not specific to aceruloplasminemia and was also described in other neurodegenerative disorders, e.g. pantothenate kinase-associated neurodegeneration (PKAN) [59].

Based on the published data [60] there is little doubt that copper, particularly that accumulated in astrocytes, is the primary toxic agent in Wilson disease. Our results suggest that iron may also contribute to astrocytic dysfunction. Nevertheless, iron-containing macrophages and astrocytes were sparse in the putamen of Wilson disease cases with mild pathological severity while large numbers were observed in cases with severe cavitation, suggesting that iron accumulation is a late event associated with tissue disruption rather than an initial factor triggering pathological changes. On the other hand, neuropathological studies are inherently biased towards more severe patients in whom treatment was unsuccessful. Our study thus serves as proof of concept while the true prevalence, extent, dynamics, and clinical correlates of iron accumulation can only be estimated from *in vivo* MRI studies.

In a SWI MRI study, signs of iron deposits in the lentiform nucleus were apparent in all Wilson disease patients with a neuropsychiatric presentation [7]. A case study of a WD patient exhibiting eye-of-the-tiger-sign, a feature fairly specific for PKAN, has also been reported [45]. Several other cross-sectional studies reported significant negative (paramagnetic) phase shift or increased susceptibility in the basal ganglia of Wilson disease patients compared to controls [10, 14, 61]. Future longitudinal studies should clarify whether iron accumulation in Wilson disease precedes neurodegenerative changes or vice versa.

In conclusion, our results provide evidence that Wilson disease with neuropsychiatric presentation is associated with iron accumulation in the brain, and that  $T_2/T_2*$  whypointensities observed *in vivo* in the deep gray matter nuclei of Wilson disease patients seem to be related to iron rather than to copper deposits. The finding of significant cerebral iron accumulation may contribute to a better understanding of Wilson disease, and may also be relevant for advances in therapeutic strategies.

# **Acknowledgments**

This work was supported by the Ministry of Health of the Czech Republic, grant nr. 15-25602A, and the Charles University in Prague, PRVOUK P26/LF1/4, as well as the Else Kröner-Fresenius Stiftung. CW was supported by the SFB TRR 43. FP was supported by the Deutsche Forschungsgemeinschaft (DFG Exc 257). VIM and JS were supported by the German Federal Ministry of Education and Research via the grant 'Center for Stroke Research Berlin' (01EO0801; http://www.bmbf.de). AC and TL were supported by grant no. N N402 471640 from the Polish Ministry of Science and Higher Education.

We would also like to acknowledge the excellent technical support by Jasmin Reichl, Angela Dettmar, Heidi Brodmerkel, Mareike Gloth and Antje Els.

**Author Contributions:** P.D., J.W., and C.W. designed the study. Data collection and analysis was performed by P.D., T.H., V.I.M., M.A.D., J.W. (MRI data); P.D., E.B., W.B. and C.W. (neuropathologic data); K.J.S., A.L., E.B. (metal analysis); T.L., and A.C. (clinical data). Data were interpreted by all authors. Figures were created by P.D., C.W., E.B., and T.H. All authors were involved in the preparation and writing of the manuscript. C.W. and J.W. are co—last authors.

#### References

- Bandmann O, Weiss KH, Kaler SG. Wilson's disease and other neurological copper disorders. Lancet Neurol 2015; 14: 103-13
- Meenakshi-Sundaram S, Mahadevan A, Taly AB, Arunodaya GR, Swamy HS, Shankar SK. Wilson's disease: a clinico-neuropathological autopsy study. J Clin Neurosci 2008; 15: 409-17
- 3 Richter R. The pallial component in hepato-lenticular degeneration. J Neuropathol Exp Neurol 1948; 7: 1-18
- 4 Schulman S, Barbeau A. Wilson's disease: a case with almost total loss of white matter. J Neuropathol Exp Neurol 1963; 22: 105-19
- 5 Bertrand E, Lewandowska E, Szpak GM, Hoogenraad T, Blaauwgers HG, Czlonkowska A, Dymecki J. Neuropathological analysis of pathological forms of astroglia in Wilson's disease. Folia Neuropathol 2001; 39: 73-9
- Sinha S, Taly AB, Prashanth LK, Ravishankar S, Arunodaya GR, Vasudev MK. Sequential MRI changes in Wilson's disease with de-coppering therapy: a study of 50 patients. Br J Radiol 2007; 80: 744-9
- 7 Skowronska M, Litwin T, Dziezyc K, Wierzchowska A, Czlonkowska A. Does brain degeneration in Wilson disease involve not only copper but also iron accumulation? Neurol Neurochir Pol 2013; 47: 542-6
- 8 Brugieres P, Combes C, Ricolfi F, Degos JD, Poirier J, Gaston A. Atypical MR presentation of Wilson disease: a possible consequence of paramagnetic effect of copper? Neuroradiology 1992; 34: 222-4
- 9 Mironov A. Decreased signal intensity of the putamen and the caudate nucleus in Wilson disease of the brain. Neuroradiology 1993; 35: 166
- Bai X, Wang G, Wu L, Liu Y, Cui L, Shi H, Guo L. Deep-gray nuclei susceptibility-weighted imaging filtered phase shift in patients with Wilson's disease. Pediatr Res 2014; 75: 436-42
- Hitoshi S, Iwata M, Yoshikawa K. Mid-brain pathology of Wilson's disease: MRI analysis of three cases. J Neurol Neurosurg Psychiatry 1991; 54: 624-6
- Maskova J, Skoloudik D, Burgetova A, Fiala O, Bruha R, Zahorakova D, Serranova T, Slovak M, Ulmanova O, Ruzicka E, Dusek P. Comparison of transcranial sonography-magnetic resonance fusion imaging in Wilson's and early-onset Parkinson's diseases. Parkinsonism Relat Disord 2016; 28: 87-93
- Engelbrecht V, Schlaug G, Hefter H, Kahn T, Modder U. MRI of the brain in Wilson disease: T2 signal loss under therapy. J Comput Assist Tomogr 1995; 19: 635-8
- 14 Fritzsch D, Reiss-Zimmermann M, Trampel R, Turner R, Hoffmann KT, Schafer A. Seven-tesla magnetic resonance imaging in Wilson disease using quantitative susceptibility mapping for measurement of copper accumulation. Investigative radiology 2014; 49: 299-306

This article is protected by copyright. All rights reserved.

2 11 12

- Kanda T, Nakai Y, Aoki S, Oba H, Toyoda K, Kitajima K, Furui S. Contribution of metals to brain MR signal intensity: review articles. Japanese journal of radiology 2016:
- Ropele S, Langkammer C. Iron quantification with susceptibility. NMR Biomed 2016:
- 17 Litwin T, Gromadzka G, Szpak GM, Jablonka-Salach K, Bulska E, Czlonkowska A. Brain metal accumulation in Wilson's disease. J Neurol Sci 2013; 329: 55-8
- 18 Cumings JN. The copper and iron content of brain and liver in the normal and in hepatolenticular degeneration. Brain 1948; 71: 410-5
- Mikol J, Vital C, Wassef M, Chappuis P, Poupon J, Lecharpentier M, Woimant F. Extensive cortico-subcortical lesions in Wilson's disease: clinico-pathological study of two cases. Acta Neuropathol 2005; 110: 451-8
- Horoupian DS, Sternlieb I, Scheinberg IH. Neuropathological findings in penicillamine-treated patients with Wilson's disease. Clin Neuropathol 1988; 7: 62-7
- Dusek P, Roos PM, Litwin T, Schneider SA, Flaten TP, Aaseth J. The neurotoxicity of iron, copper and manganese in Parkinson's and Wilson's diseases. Journal of trace elements in medicine and biology: organ of the Society for Minerals and Trace Elements 2015; 31: 193-203
- Faa G, Lisci M, Caria MP, Ambu R, Sciot R, Nurchi VM, Silvagni R, Diaz A, Crisponi G. Brain copper, iron, magnesium, zinc, calcium, sulfur and phosphorus storage in Wilson's disease. J Trace Elem Med Biol 2001; 15: 155-60
- Bruehlmeier M, Leenders KL, Vontobel P, Calonder C, Antonini A, Weindl A. Increased cerebral iron uptake in Wilson's disease: a 52Fe-citrate PET study. J Nucl Med 2000; 41: 781-7
- Ferenci P, Caca K, Loudianos G, Mieli-Vergani G, Tanner S, Sternlieb I, Schilsky M, Cox D, Berr F. Diagnosis and phenotypic classification of Wilson disease. Liver Int 2003; 23: 139-42
- Roberts EA, Schilsky ML, Diseases AAfSoL. Diagnosis and treatment of Wilson disease: an update. Hepatology 2008; 47: 2089-111
- Birkl C, Langkammer C, Haybaeck J, Ernst C, Stollberger R, Fazekas F, Ropele S. Temperature-induced changes of magnetic resonance relaxation times in the human brain: a postmortem study. Magnetic resonance in medicine 2014; 71: 1575-80
- Beyerer J, Leon FP. Suppression of inhomogeneities in images of textured surfaces. Opt Eng 1997; 36: 85-93
- Manjon JV, Coupe P, Marti-Bonmati L, Collins DL, Robles M. Adaptive non-local means denoising of MR images with spatially varying noise levels. Journal of magnetic resonance imaging 2010; 31: 192-203
- 29 Schneider CA, Rasband WS, Eliceiri KW. NIH Image to ImageJ: 25 years of image analysis. Nat Methods 2012; 9: 671-5

- Bagnato F, Hametner S, Yao B, van Gelderen P, Merkle H, Cantor FK, Lassmann H, Duyn JH. Tracking iron in multiple sclerosis: a combined imaging and histopathological study at 7 Tesla. Brain 2011; 134: 3602-15
- Meguro R, Asano Y, Odagiri S, Li C, Iwatsuki H, Shoumura K. Nonheme-iron histochemistry for light and electron microscopy: a historical, theoretical and technical review. Archives of histology and cytology 2007; 70: 1-19
- Ruifrok AC, Johnston DA. Quantification of histochemical staining by color deconvolution. Analytical and quantitative cytology and histology / the International Academy of Cytology [and] American Society of Cytology 2001; 23: 291-9
- Meguro R, Asano Y, Odagiri S, Li C, Iwatsuki H, Shoumura K. The presence of ferric and ferrous iron in the nonheme iron store of resident macrophages in different tissues and organs: histochemical demonstrations by the perfusion-Perls and -Turnbull methods in the rat. Archives of histology and cytology 2005; 68: 171-83
- Krebs N, Langkammer C, Goessler W, Ropele S, Fazekas F, Yen K, Scheurer E. Assessment of trace elements in human brain using inductively coupled plasma mass spectrometry. J Trace Elem Med Biol 2014; 28: 1-7
- Svetel M, Kozic D, Stefanova E, Semnic R, Dragasevic N, Kostic VS. Dystonia in Wilson's disease. Mov Disord 2001; 16: 719-23
- Ramos P, Santos A, Pinto NR, Mendes R, Magalhaes T, Almeida A. Anatomical region differences and age-related changes in copper, zinc, and manganese levels in the human brain. Biol Trace Elem Res 2014; 161: 190-201
- Zheng W, Monnot AD. Regulation of brain iron and copper homeostasis by brain barrier systems: implication in neurodegenerative diseases. Pharmacology & therapeutics 2012; 133: 177-88
- Gellein K, Flaten TP, Erikson KM, Aschner M, Syversen T. Leaching of trace elements from biological tissue by formalin fixation. Biol Trace Elem Res 2008; 121: 221-5
- Hallgren B, Sourander P. The effect of age on the non-haemin iron in the human brain. J Neurochem 1958; 3: 41-51
- 40 Gossuin Y, Gillis P, Muller RN, Hocq A. Relaxation by clustered ferritin: a model for ferritin-induced relaxation in vivo. NMR Biomed 2007; 20: 749-56
- Wender M, Adamczewska Z, Gruszczynska U, Dezor A. The cerebral copper-protein complexes in hepato-lenticular degeneration studied by means of electron-spin-resonance technique. Acta Neurol Scand 1974; 50: 812-5
- Tapia L, Gonzalez-Aguero M, Cisternas MF, Suazo M, Cambiazo V, Uauy R, Gonzalez M. Metallothionein is crucial for safe intracellular copper storage and cell survival at normal and supraphysiological exposure levels. Biochem J 2004; 378: 617-24

- 43 Morris CM, Candy JM, Oakley AE, Bloxham CA, Edwardson JA. Histochemical distribution of non-haem iron in the human brain. Acta anatomica 1992; 144: 235-57
- 44 Connor JR, Menzies SL, St Martin SM, Mufson EJ. Cellular distribution of transferrin, ferritin, and iron in normal and aged human brains. J Neurosci Res 1990; 27: 595-611
- Litwin T, Karlinski M, Skowronska M, Dziezyc K, Golebiowski M, Czlonkowska A. MR image mimicking the "eye of the tiger" sign in Wilson's disease. J Neurol 2014; 261: 1025-7
- Dusek P, Jankovic J, Le W. Iron dysregulation in movement disorders. Neurobiology of disease 2012; 46: 1-18
- 47 Rouault TA. Iron metabolism in the CNS: implications for neurodegenerative diseases. Nat Rev Neurosci 2013; 14: 551-64
- 48 Reddy PV, Rao KV, Norenberg MD. The mitochondrial permeability transition, and oxidative and nitrosative stress in the mechanism of copper toxicity in cultured neurons and astrocytes. Lab Invest 2008; 88: 816-30
- Simmons DA, Casale M, Alcon B, Pham N, Narayan N, Lynch G. Ferritin accumulation in dystrophic microglia is an early event in the development of Huntington's disease. Glia 2007; 55: 1074-84
- Kwan JY, Jeong SY, Van Gelderen P, Deng HX, Quezado MM, Danielian LE, Butman JA, Chen L, Bayat E, Russell J, Siddique T, Duyn JH, Rouault TA, Floeter MK. Iron accumulation in deep cortical layers accounts for MRI signal abnormalities in ALS: correlating 7 tesla MRI and pathology. PLoS One 2012; 7: e35241
- Andersen HH, Johnsen KB, Moos T. Iron deposits in the chronically inflamed central nervous system and contributes to neurodegeneration. Cell Mol Life Sci 2014; 71: 1607-22
- Davies KM, Hare DJ, Cottam V, Chen N, Hilgers L, Halliday G, Mercer JF, Double KL. Localization of copper and copper transporters in the human brain. Metallomics 2013; 5: 43-51
- Hayashi H, Yano M, Fujita Y, Wakusawa S. Compound overload of copper and iron in patients with Wilson's disease. Med Mol Morphol 2006; 39: 121-6
- Boaru SG, Merle U, Uerlings R, Zimmermann A, Flechtenmacher C, Willheim C, Eder E, Ferenci P, Stremmel W, Weiskirchen R. Laser ablation inductively coupled plasma mass spectrometry imaging of metals in experimental and clinical Wilson's disease. J Cell Mol Med 2015; 19: 806-14
- Pfeiffenberger J, Gotthardt DN, Herrmann T, Seessle J, Merle U, Schirmacher P, Stremmel W, Weiss KH. Iron metabolism and the role of HFE gene polymorphisms in Wilson disease. Liver Int 2012; 32: 165-70
- Medici V, Di Leo V, Lamboglia F, Bowlus CL, Tseng SC, D'Inca R, Irato P, Burra P, Martines D, Sturniolo GC. Effect of penicillamine and zinc on iron metabolism in Wilson's disease. Scand J Gastroenterol 2007; 42: 1495-500

- Morita H, Ikeda S, Yamamoto K, Morita S, Yoshida K, Nomoto S, Kato M, Yanagisawa N. Hereditary ceruloplasmin deficiency with hemosiderosis: a clinicopathological study of a Japanese family. Ann Neurol 1995; 37: 646-56
- Kaneko K, Yoshida K, Arima K, Ohara S, Miyajima H, Kato T, Ohta M, Ikeda SI. Astrocytic deformity and globular structures are characteristic of the brains of patients with aceruloplasminemia. J Neuropathol Exp Neurol 2002; 61: 1069-77
- Kruer MC, Hiken M, Gregory A, Malandrini A, Clark D, Hogarth P, Grafe M, Hayflick SJ, Woltjer RL. Novel histopathologic findings in molecularly-confirmed pantothenate kinase-associated neurodegeneration. Brain 2011; 134: 947-58
- Scheiber IF, Dringen R. Astrocyte functions in the copper homeostasis of the brain. Neurochemistry international 2013; 62: 556-65
- Yang J, Li X, Yang R, Yu X, Yu C, Qian Y, Yu Y. Susceptibility-Weighted Imaging Manifestations in the Brain of Wilson's Disease Patients. PLoS One 2015; 10: e0125100

# Figure legends

- **Fig.1** Correlation of T2/T2\*w hypointensity on MRI and iron staining in the basal ganglia in control and neuro-WD subjects
- A, C, E) coronal MP-RAGE MR images (TR=2300 ms, TE=5.9 ms) at the level of the basal ganglia. A) Control case with a slightly lower signal in the globus pallidus (black arrowhead) compared to the putamen (empty arrowhead) and the caudate nucleus (arrow). C) Neuro-WD with moderate disease severity (case 4) and with pronounced hypointensity in the globus pallidus (black arrowhead) and the subthalamic nucleus/substantia nigra region (white arrowhead). Milder hypointensity is present in the putamen (empty arrowhead) and the caudate nucleus (arrow). E) Severe neuro-WD (case 5) with pronounced hypointensity in the caudal part of the putamen (arrowhead) and lateral part of the globus pallidus and mild hypointensity in the caudate nucleus (arrow). Asterisks denote the anterior commissure.
- B, D, F) Low power magnification of the basal ganglia (corresponding to areas marked by orange rectangles on MR images) stained by Turnbull iron staining. B) Control case with normal pattern of iron staining, i.e. diffuse staining in the globus pallidus and weaker staining in the putamen, where iron is present mostly in myelinated bundles (arrows). D) Diffuse iron staining in the lentiform nucleus that is stronger in the globus pallidus than in the putamen, in correspondence with the MR signal. Note that myelinated bundles are still detectable (arrows) within diffusely increased iron staining. F) Strong diffuse iron staining in lentiform and caudate nuclei; the area of low MR signal in the caudal putamen corresponds to the area of rarefied and profoundly disrupted tissue (dashed circle). Note the disrupted structure of iron-containing myelinated bundles in the putamen, while these are preserved in the caudate nucleus (arrows); asterisks denote the anterior commissure.

Fig.2 Iron accumulation in the putamen in neuro-WD

A) Corresponding MP-RAGE (TR=2300 ms, TE=5.9 ms) MRI and B) low power magnification of the Turnbull iron staining displaying the corresponding area in the putamen (dashed circles) also shown in high power images for different stainings C-H (MRI and all histological images from neuro-WD case 5). C) Turnbull iron staining shows tissue disruption and granular, dense iron deposits in macrophages (orange arrows) and a few enlarged reactive astrocytes (black arrow). D) Ferritin staining matches well with the Turnbull staining and shows numerous strongly positive macrophages (orange arrows) and faint staining in a few astrocytes (black arrow). E-F) Two exemplary pictures of HE-stained putamen showing tissue rarefaction and spongious degeneration with numerous macrophages (E) and astrogliosis (F); black arrows denote reactive astrocytes, arrowheads denote exemplary macrophages. G) Double staining for Turnbull iron (red) and KiM1P (blue) showing double stained cells representing iron-containing macrophages (orange arrows). Note that several apparently extracellular iron deposits are found in cells with round shape and foamy appearance with a morphology resembling macrophages (orange arrowheads). H) Double staining for Turnbull iron (red) and GFAP (blue) showing double-stained cells representing iron-containing astrocytes (black arrows). Note that iron is not only associated with astrocytes but is also deposited in a perivascular round cell without GFAP staining most likely to be a macrophage (orange arrow). A few astrocytes are negative for Turnbull iron staining (black arrowheads). Scale bars represent 5 mm (B) or 50 μm (C-H).

**Fig.3** Correlation between R<sub>2</sub>\* value, density of iron staining and metal concentration in Wilson disease cases

Graphs show data for the GP, putamen, and caudate nucleus. In the upper row, Y axes indicate the proportion of tissue with positive Turnbull signal in % as a measure of iron staining density. The  $R_2$ \* value is significantly correlated with the density of iron staining in the globus pallidus (A) and putamen (B); no correlation was observed in the caudate nucleus (C).

In the middle and bottom rows, Y axes indicate the concentration of metals in  $\mu g/g$ , whereby the correlations of iron (Fe) concentration and  $R_2^*$  value is shown in the middle row and the correlation of copper (Cu) concentration and  $R_2^*$  is given in the bottom row. The  $R_2^*$  value is significantly correlated with the iron concentration in the globus pallidus (D), putamen (E) and caudate nucleus (F) while it is not correlated with the copper concentration in any of the examined areas (G-I).

Fig.4 Mean cerebral concentration of iron and copper in Wilson disease cases and controls

Y axes indicates the concentration of metals in  $\mu g/g$ , whereby the results for iron (Fe) are shown in the left graph, and the results for copper (Cu) are given in the right graph for different areas of the brain. Note that the scales of Y axes are different for both metals. Bars indicate mean metal concentrations in neuro-WD (grey bars) and control (black bars) cases. Diamonds represent iron and copper concentrations in individual hepato-WD cases whose values are not included in the bars.

<sup>\*</sup> p<0.05, error bars denote SD.

**Fig.5** Increased phagocytic and astrocytic iron deposits in the putamen of cases with severe Wilson disease pathology

A) The number of KiM1P+ cells positive for iron in samples with mild (none or mild tissue disruption) and severe (moderate or severe tissue disruption) pathology in the putamen. B) Positive correlation between iron concentration and the number of KiM1P+ cells positive for iron. C) The number of GFAP+ cells positive for iron in samples with mild and severe pathology in the putamen. D) Positive correlation between iron concentration and number of GFAP+ cells positive for iron.

\* p<0.05, error bars denote SD.

 Table 1. Clinical characteristics of patient cases

Case number	Sex	Age at death (yrs)	Disease duration (yrs)	Neuropsychiatric symptoms	Liver symptoms	Diagnostic findings	Treatment	Treatment duration (months)	Cause of death	Fixation duration (yrs)	Postmortem interval (hrs)
1	М	35	2	At onset: tremor subtype At progression: choreodystonia	Cirrhosis	KF ring, Cp 8.7mg/dl	Zinc	13	Pneumonia, cachexia	21	24
2	М	33	1	At onset: tremor subtype At progression: mania and generalized dystonia	Cirrhosis	KF ring, Cp 11.1mg/dl	D-PNC, BAL	10	Pneumonia	16	24
3	М	22	4	At onset: tremor subtype with mania At progression: generalized dystonia	Cirrhosis	KF ring, Cp 0.8mg/dl	D-PNC	5	Pneumonia	16	24
4	F	41	2	At onset: tremor subtype At progression: generalized dystonia	Cirrhosis	Cp 14.1.mg/dl, urine Cu excretion 56μg/24h	Zinc, D-PNC	3	Sepsis, DIC	16	48
5	F	42	4	At onset: parkinsonism subtype with depression At progression: generalized dystonia	Cirrhosis	KF ring, Cp 13.8mg/dl, urine Cu excretion 217μg/24h	D-PNC	8	Pneumonia	15	24

This article is protected by copyright. All rights reserved.

	Abl
	coa
	Th

6	F	31	1	At onset: tremor subtype with anarthria At progression: moderate dystonia	Cirrhosis	KF ring, Cp 12mg/dl, homozygous p.H1069Q mutation	D-PNC	12	Sepsis, DIC	8	48
7	М	21	1	At onset: dystonic subtype At progression: generalized dystonia with mania	Cirrhosis	KF ring, Cp 2.2mg/dl, homozygous p.G1186C mutation	D-PNC, Zinc	5	Pneumonia, sepsis, cachexia	7	12
8	F	35	0.5	None	Acute liver failure	Cp 6.5mg/dl, urine Cu excretion 1650μg/24h	None	0	Acute liver failure	19	300
9	F	22	7	None	Acute liver failure	N/A	LTX 2006 and reLTX 2013	N/A	Acute liver failure, sepsis	0.6	24

Abbreviations: M – male, F – female, N/A – not available, yrs – years, Cp – ceruloplasmin (normal range: 20 - 50 mg/dl), Cu excretion – daily urinary copper excretion (normal range: 0–50 μg/24 hours), KF ring – Keyser-Fleischer ring, D-PNC – D-penicillamine, LTX - orthotopic liver transplantation, DIC – disseminated intravascular coagulopathy

This article is protected by copyright. All rights reserved.

Table 2. Characteristics of control cases

Case numbe r	Se x	Medical history	Age at deat h (yrs)	Cause of death	Fixatio n duratio n (yrs)	Postmorte m interval (hours)	Putame n Iron (µg/g)	Putame n Copper (µg/g)	Globus Pallidu s Iron (µg/g)	Globus Pallidu s Coppe r (µg/g)
1	М	None	37	Multiple injury without head involveme nt	4	48	37.1	1.35	64.2	2.41
2	M	N/A	61	Cardiac tamponad e/ aortal dissection	1	48	38.9	3.09	58.4	4.54
3	M	N/A	56	Cardiac infarction	1	120	104	6.56	86.5	4.64
4	F	N/A	34	N/A	3	24	80.2	4.75	148	5.98
5	F	Atrial fibrillation anticoagulatio n	56	N/A	1	48	46.4	3	75.8	3.68
6	F	Carcinoma of the rectum, renal failure	53	Sepsis	1	36	50.2	4.5	102	5.04

Abbreviations: M – male, F – female, N/A – not available, yrs – years

 Table 3. Descriptive and quantitative neuropathological findings in Wilson disease cases

	Des	Putamen					Globus pallidus						
Case num ber	Cortical areas	Brainstem	Basal ganglia	Tissue disrup tion	GFA P+ cells posit ive for Fe (per mm²	KiM 1P+ cells posit ive for Fe (per mm² )	lro n (μg /g)	Cop per (µg/ g)	Tissue disrup tion	GFA P+ cells posit ive for Fe (per mm²	KiM 1P+ cells posit ive for Fe (per mm² )	lro n (μg /g)	Cop per (µg/ g)
1	Inconspi cuous	Three microscopic necrotic lesions (infarction) in pons	Putamin al cavitatio n; severe astroglio sis; medium neuronal loss; numero us macroph ages; loss of myelinat ed bundles in GP	+++	48	136	107	8.6	++	16	32	91.	12.1
2	Inconspi cuous	Two microscopic microhemor rhages in pons; mild spongiosis in SN	Putamin al cavitatio n; severe astroglio sis; medium neuronal loss; numero us macroph ages; loss of myelinat ed bundles in GP	+++	32	120	70. 3	11.8	+	0	136	93. 1	12.6
3	Inconspi cuous	Inconspicuo us (SN N/A)	Mild astroglio sis, loss of	+	16	80	93. 2	17.9	+	24	16	110	31.5

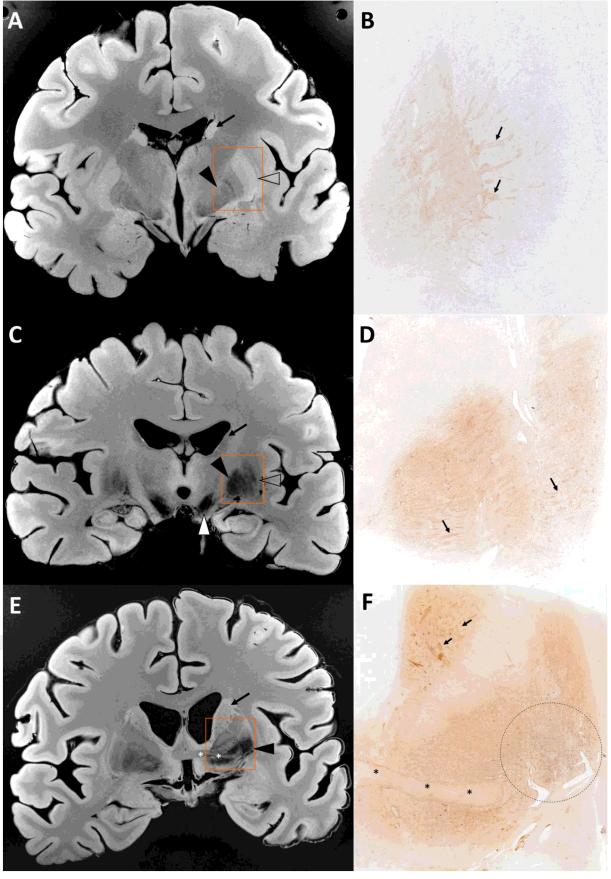
_							T							
				myelinat ed bundles, medium neuronal loss, few macroph										
	4	Mild astroglio sis	Mild spongiosis in SN, mild astrogliosis	ages Mild astroglio sis, few macroph ages	0	0	56	103	32.5	0	0	40	101	39
	5	Inconspi cuous	Mild spongiosis with small superposed cavitation in SN, mild astrogliosis	Focal putamin al cavitatio n; severe astroglio sis; medium neuronal loss, numero us macroph ages	++	40	176	149	36.4	+	16	40	182	46.7
	6	Inconspi cuous	Mild spongiosis in SN, mild astrogliosis	Mild astroglio sis	0	0	16	68. 1	19.9	0	0	0	109	42.7
	7	Pronoun ced astroglio sis	N/A	Severe putamin al cavitatio n and shrinkag e; severe astroglio sis; severe neuronal loss in putamen ; numero us macroph ages	+++	16	136	105	13.7	+	8	96	64. 6	53.1
	8	Mild astroglio sis	Mild spongiosis in SN, mild astrogliosis	Mild astroglio sis	0	0	0	21. 5	4.1	0	0	0	35. 3	16.2
	9	Inconspi cuous	Inconspicuo us	Mild astroglio sis	0	0	0	26. 2	18.5	0	0	0	49. 8	17.3

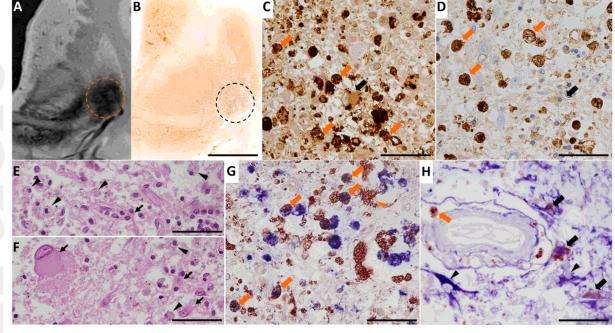
Wilson disease cases with hepatic presentation are highlighted in grey color. Abbreviations: SN - substantia nigra, N/A - not available

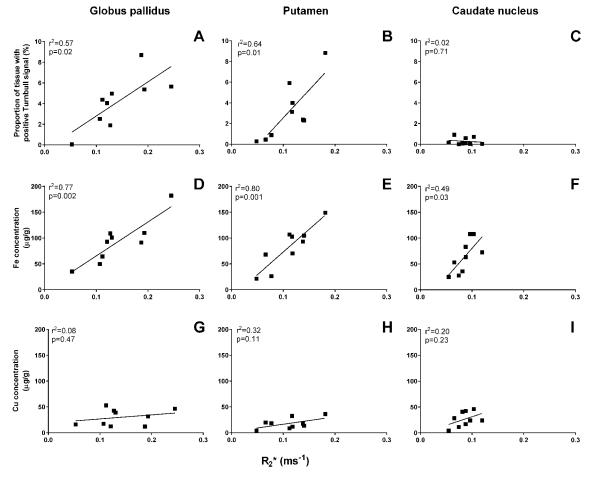
**Table 4.** Coefficients of multiple regression models of R2\* value in the basal ganglia based on iron (Model 1) and iron and copper (Model 2) concentrations

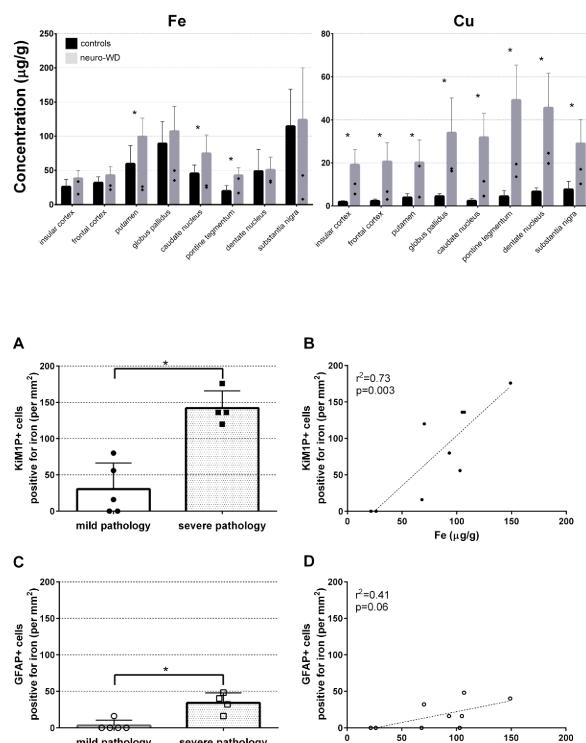
	В	SE B	β
Model 1			
Constant	0.033	0.012	
Iron	0.001	0.0001	0.837*
Model 2			
Constant	0.033	0.013	
Iron	0.001	0.0001	0.844*
Copper	-0.0001	0.0004	-0.015

B = unstandardized coefficient, SE = standard error of mean,  $\beta$  = standardized coefficient Note:  $r^2$ =0.70 for Model 1;  $\Delta r^2$ = 0.0002 for Model 2 (p=0.9); \*p<0.0001









100

Fe (µg/g)

50

severe pathology

mild pathology